Dual Nuclear Product Observations of Shock Collapse in Inertial Confinement Fusion

The speed and heating of convergent shocks are of fundamental importance for the design of high-gain implosions in inertial confinement fusion (ICF).[1,2] Strong, spherically convergent shocks are formed by the rapid deposition of energy in the form of lasers (direct drive) or x rays (indirect drive) on the surface of a spherical capsule. Current ICF ignition designs include a sequence of up to four convergent shocks that must be precisely timed to coalesce at the inner shell surface in order to obtain maximal shell compression,[3,4] a necessity for high fusion gain. All shocks formed after the first must propagate through hot, already-shocked material, which introduces uncertainty into the shock speed and strength. A thorough understanding of shock speeds in cold and heated material, and in planar and convergent geometries, will be vital for satisfactory ICF implosion performance.

Previous studies of shock propagation relevant to ICF have focused largely on planar geometry.[5,6] The planar approximation works well for the propagation of converging shocks in the shell at early times, but it breaks down as the shock approaches the center of collapse. Nuclear measurements of some aspects of shock collapse using a single nuclear product have also recently been reported.[7,8]

This article presents the first results of temporal and spectral measurements of products from two nuclear reaction types induced by the central collapse of convergent shocks. Observations of these products provide information about the speed and heating of the shocks, as well as the state of the imploding capsule at the time of shock collapse, which, in the experiments discussed here, occurs immediately before the onset of the deceleration phase and the final stages of compression. The dual nuclear reaction measurements act as a powerful constraint and verification of observable and inferred values of shock collapse.

Direct-drive implosions were conducted on the OMEGA laser[9] with 60 beams of ultraviolet (351 nm) light in a 1-ns flattop pulse, a total energy of 23 kJ, and full single-beam smoothing.[10] The spherical capsules had diameters between 860 and 880 μm, plastic (CH) shell thicknesses of 20, 24, or 27 μm, and a flash coating of 0.1 μm of aluminum. The capsules were filled with an equimolar (by atom) mixture of D_2 and ^{3}He gas with a total fill pressure (P_0) of 3.6 or 18 atm at 293 K, corresponding to initial fill mass densities of 0.5 and 2.5 mg/cm^3, respectively.

Three distinct primary nuclear reactions proceed during capsule implosions with D_2 and ^{3}He fuel: $D + D \rightarrow {}^3He + n$; $D + D \rightarrow T + p$; and $D + {}^3He \rightarrow {}^4He + p$. The neutron and proton branches of the D-D reaction have nearly equal probabilities over temperatures of interest. The D-^{3}He reaction depends much more strongly on temperature due to the doubly charged ^{3}He reactant.[11]

Nuclear products were observed by using the proton and neutron temporal diagnostics (PTD and NTD)[8,12] to measure the D-^{3}He and DD-*n* reaction histories; multiple wedged-range-filter (WRF) proton spectrometers[13] to measure the D-^{3}He proton yield and spectrum; and a magnet-based charged-particle spectrometer[13] to measure D-D protons emitted at shock-bang time. The birth energies of D-^{3}He and D-D protons are 14.7 and 3.0 MeV, respectively.

Experimental results were compared with numerical simulations performed using *LILAC*,[14] a one-dimensional (1-D) Lagrangian hydrodynamic code, which includes laser-beam ray-tracing, a tabular equation of state, and multigroup diffusion radiation transport. The electron thermal energy is transported using a flux-limited diffusion model in which the effective energy flux is defined as the minimum of the diffusion flux and a fraction f of the free-streaming flux. The flux limiter $f = 0.06$ unless otherwise specified.

The D-^{3}He reaction rate history shows two distinct times of nuclear production [Fig. 111.14(a)]: "shock burn" begins shortly after shock collapse and ends near the beginning of the deceleration phase; "compression burn" begins near the onset of the deceleration phase and lasts approximately until stagnation of the imploding shell. For ordinary D^{3}He mixtures, the DD-*n*

reaction rate during the shock burn is below the diagnostic detection threshold.

The shock and compression components can often be distinguished in D^3He proton spectra [Fig. 111.14(b)].[7] The protons emitted at shock-bang time experience relatively little downshift (~0.4 MeV) due to the low total capsule areal density (ρR) at that time. The shell continues to compress after shock burn ends, and by compression-bang time the ρR has increased enough to downshift the D^3He protons by several MeV.

The ρR during the shock burn is low enough to also allow nascent 3.0-MeV DD protons to escape the capsule [Fig. 111.14(c)]. Measurement of DD protons emitted during shock burn provides a valuable and sole measurement of the D-D shock yield when the reaction rate is below the NTD threshold. Measurement of their downshift can also provide a double check on the ρR at shock-bang time inferred using the D^3He proton spectra, or the sole measurement in cases where the shock component of the D^3He proton spectrum cannot be separated from the compression component.

Observed and simulated shock-bang times and D-^{3}He and DD-p shock yields are shown in Fig. 111.15 as functions of shell thickness for implosions of capsules with different P_0. The shock-bang time is the time of peak D-^{3}He nuclear production during the shock-burn phase, the D-^{3}He shock yield includes only the contribution from the higher-energy "shock" component of the D^3He-proton spectrum, and the DD-p shock yield includes only that part of the spectrum above the high-energy cutoff of ablator protons[15] [seen at 0.8 MeV in Fig. 111.14(c)]. The figure plots the mean and the standard error of the mean for shot ensembles of each capsule configuration. Summaries of experimental results are included in Tables 111.I and 111.II.

Experiments show that shock-bang time is linearly delayed with increasing shell thickness [Fig. 111.15(a)], corresponding to a shock speed of ~30 km/s in the shell. No difference in shock-bang time was observed for capsules with different P_0. Simulations predict shock-bang time to occur much later than is consistent with experiments,[16] as well as a strong dependence on fill pressure.

Observations show that both D-^{3}He and D-D shock yields decrease for implosions of targets with thicker shells and lower P_0. The reduction factor for lower fill pressures has a lower value (3 to 5), however, than that expected (25) due only to the density dependence of the nuclear fusion rate; the lower density also results in less-efficient thermal coupling between ions and electrons, so that the ion temperature, and consequently the nuclear fusion rate, stays higher.

The average ion temperature at shock-bang time $\langle T_i \rangle_{sh}$ can be inferred using the measured yields of the two different nuclear reactions, based on the ratio of their respective thermal reactivities.[17] Figure 111.16 demonstrates the anticipated higher $\langle T_i \rangle_{sh}$ for 3.6-atm implosions. The shock temperature of 5.4±0.4 keV for 24-μm-thick, 18-atm implosions compares favorably with the value of 6±1 keV obtained by a fit to the shock line width, assuming only thermal broadening, reported by Petrasso *et al.*[7]

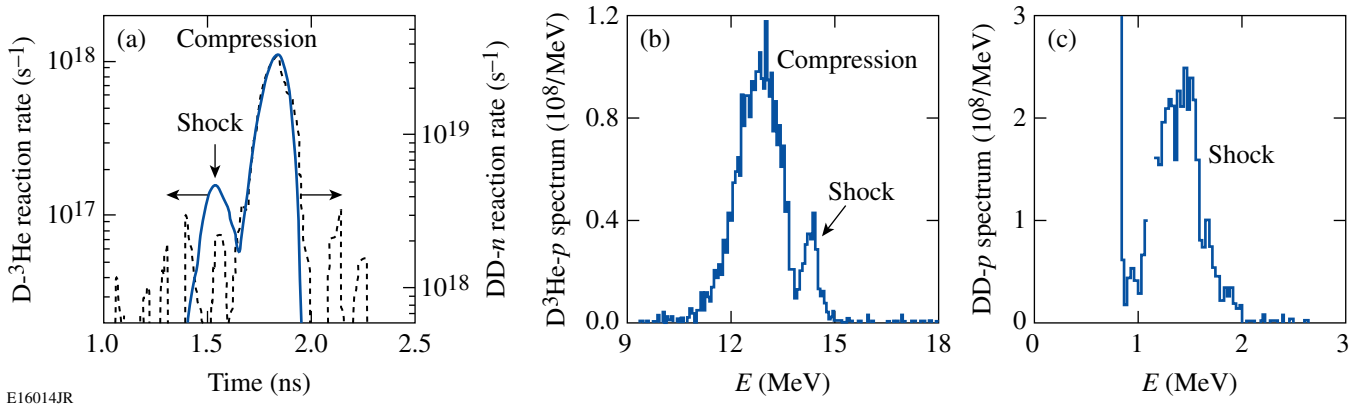

Figure 111.14
Representative experimental observations of D-D and D-^{3}He nuclear products emitted at shock- and compression-bang time from an implosion of a 24-μm-thick CH capsule shell filled with 18 atm of D^3He gas (OMEGA shot 38525). (a) D-^{3}He (solid) and DD-n (dashed) reaction rate histories; (b) D^3He-proton spectrum; (c) DD-proton spectrum.

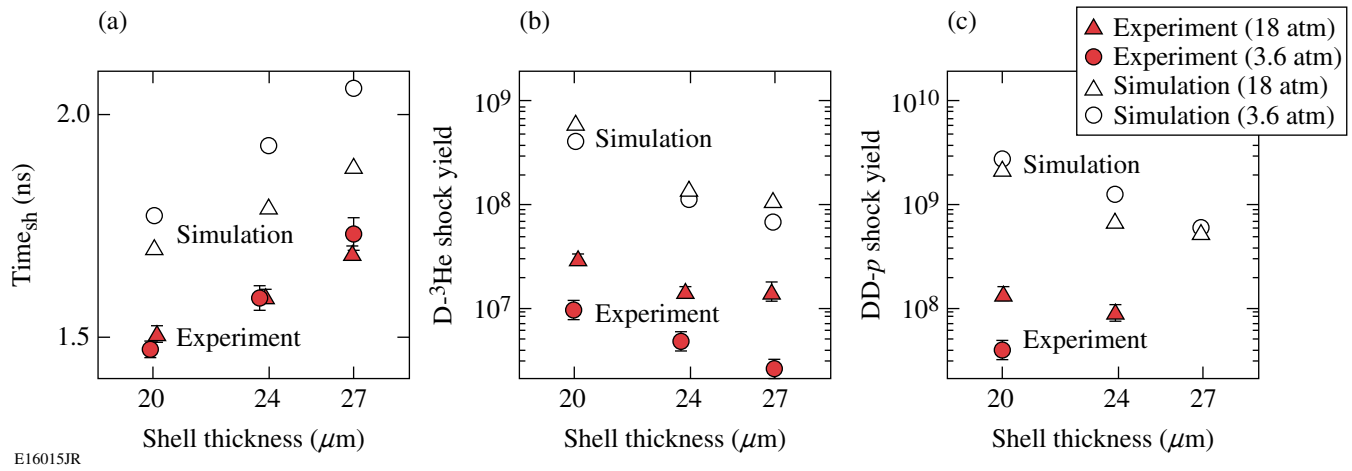

Figure 111.15
Experimental observations (solid) and 1-D simulations (open) of (a) shock-bang time, (b) D-^{3}He shock yield, and (c) DD-p shock yield as a function of capsule shell thickness for ensembles of capsules filled with 18 atm (triangles) or 3.6 atm (circles) of D^{3}He gas.

Table 111.I: Mean and error of measured values of shock-bang time, D-^{3}He shock yield, and ρR at shock time for implosions with different shell thicknesses and fill pressures. The D-^{3}He shock yield is shown as both an absolute yield and a percentage of the total D-^{3}He yield.

P (atm)	ΔR (μm)	N	t_{sh} (ps)	$Y_{p\text{-}s}$ ($\times 10^7$)	err (%)	$Y_{p\text{-}s}$ (% Y_p)	ρR (mg/cm^2)
3.6	19.9	8	1470±16	—	—	—	—
3.6	23.7	6	1585±27	0.48	9	10.6±0.9	9.8±0.4
3.6	27.0	4	1731±39	0.25	20	12.2±1.7	12.0±0.9
18	20.1	8	1506±16	3.09	7	6.2±0.5	8.2±1.0
18	23.9	9	1591±12	1.45	9	9.3±0.6	8.9±0.7
18	26.9	6	1690±11	1.44	18	19.8±2.5	9.4±1.2

Table 111.II: Mean and error of measured values of DD-p shock yield, shock T_i, and ρR at shock time inferred from the downshift of DD-p, for implosions with different shell thicknesses and 18-atm fill pressure. The DD-p shock yield is shown as both an absolute yield and a percentage of the total DD-n yield.

P (atm)	ΔR (μm)	N	$\langle T_i \rangle_{sh}$ (keV)	$Y_{DD\text{-}s}$ ($\times 10^7$)	err (%)	$Y_{DD\text{-}s}$ (% Y_n)	ρR (mg/cm^2)
3.6	19.9	5	7.9±0.9	4.2	10	1.5±0.2	8.3±0.7
18	20.2	3	5.9±0.4	14.1	13	1.2±0.2	9.3±0.6
18	23.9	3	5.4±0.4	9.2	20	1.9±0.3	10.0±0.7
18	27.1	2	—	—	—	—	11.1±1.0

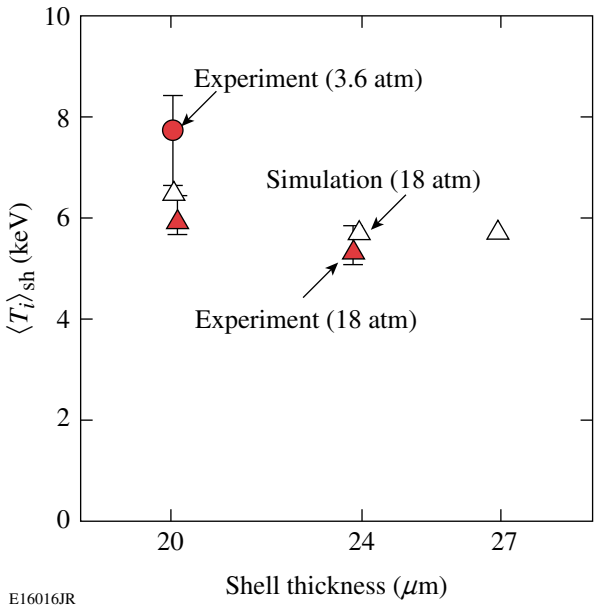

Figure 111.16
Shock-burn–averaged ion temperature, calculated using the ratio of the DD-p to D-^{3}He shock yields from experiments (solid) and from 1-D simulations (open) for capsules filled with 18 atm (triangles) and 3.6 atm (circles) of D^{3}He gas.

One-dimensional simulations grossly overestimate the experimentally observed D-^{3}He and DD-p shock yields. The experimental yield over the calculated yield (YOC) is 3%–4% for 3.6-atm fills and 5%–15% for 18-atm fills. These higher predicted yields combined with only slightly higher values of $\langle T_i \rangle_{sh}$ indicate that simulations calculate that, compared to experiment, capsules at shock-bang time are more highly compressed.

The compression of the capsule at shock-bang time can be quantified by the shock-burn–averaged areal density, ρR_{sh}. Experimentally, ρR_{sh} is inferred from the measured mean energy downshift from the birth energy of DD protons or D^{3}He protons in the shock line, using a theoretical formalism to relate their energy loss to plasma parameters.[13,18] The inferred ρR_{sh} value is insensitive to the exact values assumed, particularly when using the downshift of 14.7-MeV protons; a CH plasma density of 3 g/cm^3 and a temperature of 0.3 keV were used to derive the quoted ρR_{sh} values. The simulated ρR_{sh} is calculated as the ρR weighted by the D-^{3}He reaction rate over the shock burn.

Excellent agreement is observed between ρR_{sh} inferred from spectral results obtained using both DD and D^{3}He protons, as shown in Fig. 111.17 and Tables 111.I and 111.II. Compared to

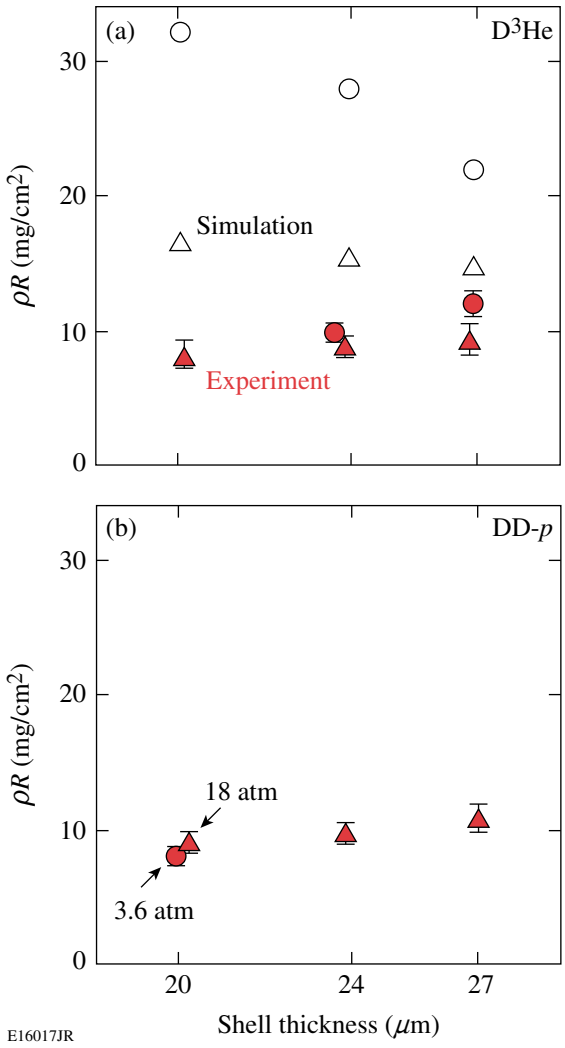

Figure 111.17
Shock ρR's for 18-atm (triangles) and 3.6-atm (circles) D^{3}He fills of capsules as functions of shell thickness. The experimental ρR_{sh} is inferred from the downshift of nascent (a) 14.7-MeV D^{3}He protons and (b) 3-MeV DD protons from their birth energy. Markers show mean and standard error. The simulated ρR [open markers in (a)] is the ρR of the implosion weighted by the D-^{3}He reaction rate over the shock burn.

experiments, 1-D simulations predict much higher ρR_{sh} and show an opposing trend of ρR_{sh} as a function of shell thickness and a very strong dependence of ρR_{sh} on P_0. A higher predicted ρR_{sh} is consistent with the expectation of higher compression discussed above.

On the basis of physical principles, ρR_{sh} should be nearly independent of P_0 since the trajectory of the shell will not be affected by the fill gas until the deceleration phase, well after shock-bang time. Scrutiny of the simulated reaction rate histo-

ries for low-P_0 implosions reveals additional nuclear production caused by a reflection of the outgoing shock from the imploding shell. This shock reverberation explains the larger discrepancy for the yields, shock-bang times, and ρR_{sh}'s seen for low-P_0 simulations; however, no evidence of heating due to the shock reverberation is seen in the observed reaction rates.

Several competing shell-thickness–dependent effects could alter ρR_{sh}. For the same laser drive, the same amount of shell mass gets ablated, which for thicker shells results in more remaining mass (which tends to increase ρR_{sh}) and lower implosion velocity (which tends to decrease ρR_{sh}). The opposing trends of ρR_{sh} with shell thickness for experiments and simulations demonstrate that the simulations are improperly treating these competing effects.

The overprediction of shock yields, ρR_{sh}'s, and time until shock collapse by 1-D simulations might at first indicate the need for 2-D or 3-D simulations to capture the complete physics of collapsing shocks. Indeed, theoretical analysis suggests that converging shocks are weakly unstable to initial asymmetries;[19] however, experiments have demonstrated that the observables are highly robust to drive asymmetries[20] and that the growth of asymmetries due to hydrodynamic instabilities is insufficient to mix the shell with the fill gas at shock collapse time.[21] The collapse and resulting nuclear production of converging shocks can thus be well approximated as a 1-D situation; more computationally intensive 2-D or 3-D simulations are unnecessary.

One-dimensional simulations can be adjusted to match experimental timing by increasing the flux limiter f; however, increasing f will also push the shock yield and ρR into further disagreement with experiments. No value of the flux limiter can match both the shock timing and yield simultaneously, suggesting a limitation of handling shock collapse using only a hydrodynamic treatment. The fuel plasma during the shock burn is hotter and sparser than it is during the compression burn, which results in lower collision frequency and ion mean free paths that are comparable to the size of the plasma. Comparison of hydrodynamic and kinetic simulations[22] shows that the kinetic treatment results in a weaker reflected shock and a nuclear production substantially lower during the shock burn.

In summary, nuclear production induced by the collapse of strong, spherically convergent shocks was observed using temporal and spectral measurements of products from two distinct nuclear reactions. The dual nuclear observations create a comprehensive description of the state of the implosion at shock-collapse time, which, temporal measurements show, occurs immediately before the onset of the deceleration phase. Measuring both DD and D^3He nuclear products acts as a powerful constraint and verification of data reliability; observations of their yields and spectra are used to infer temperatures and areal densities at shock-bang time near 6 keV and 10 mg/cm^2, respectively. Comparison of the experimental results to predictions made by 1-D hydrodynamic simulations revealed numerous differences, including earlier time of shock collapse, lower nuclear production and fill-gas temperature, and lower capsule compression at shock-bang time. Given the importance of shock timing and heating to the success of ignition in ICF, it is worthwhile to re-examine the treatment of shocks in current hydrodynamic codes; the constraints imposed by this compelling set of dual nuclear shock-burn measurements make it possible for efficient and insightful alterations to be selectively made in ICF simulations at a level hitherto unavailable.

ACKNOWLEDGMENT

The authors express their gratitude to the OMEGA engineers and operations crew who supported these experiments. This work was supported in part by the U.S. Department of Energy Office of Inertial Confinement Fusion (Grant No. DE-FG03-03NA00058), by the Fusion Science Center for Extreme States of Matter and Fast Ignition (Contract No. 412761-G), by the Laboratory for Laser Energetics (Subcontract No. 412160-001G), and by the Lawrence Livermore National Laboratory (Subcontract No. B543881).

REFERENCES

1. J. Nuckolls *et al*., Nature **239**, 139 (1972).

2. S. Atzeni and J. Meyer-ter-Vehn, *The Physics of Inertial Fusion: Beam Plasma Interaction, Hydrodynamics, Hot Dense Matter*, International Series of Monographs on Physics (Clarendon Press, Oxford, 2004).

3. D. H. Munro *et al*., Phys. Plasmas **8**, 2245 (2001).

4. R. L. McCrory, R. E. Bahr, R. Betti, T. R. Boehly, T. J. B. Collins, R. S. Craxton, J. A. Delettrez, W. R. Donaldson, R. Epstein, J. Frenje, V. Yu. Glebov, V. N. Goncharov, O. Gotchev, R. Q. Gram, D. R. Harding, D. G. Hicks, P. A. Jaanimagi, R. L. Keck, J. Kelly, J. P. Knauer, C. K. Li, S. J. Loucks, L. D. Lund, F. J. Marshall, P. W. McKenty, D. D. Meyerhofer, S. F. B. Morse, R. D. Petrasso, P. B. Radha, S. P. Regan, S. Roberts, F. Séguin, W. Seka, S. Skupsky, V. Smalyuk, C. Sorce, J. M. Soures, C. Stoeckl, R. P. J. Town, M. D. Wittman, B. Yaakobi, and J. D. Zuegel, Nucl. Fusion **41**, 1413 (2001).

5. T. R. Boehly, E. Vianello, J. E. Miller, R. S. Craxton, T. J. B. Collins, V. N. Goncharov, I. V. Igumenshchev, D. D. Meyerhofer, D. G. Hicks, P. M. Celliers, and G. W. Collins, Phys. Plasmas **13**, 056303 (2006).

6. V. N. Goncharov, O. V. Gotchev, E. Vianello, T. R. Boehly, J. P. Knauer, P. W. McKenty, P. B. Radha, S. P. Regan, T. C. Sangster, S. Skupsky, V. A. Smalyuk, R. Betti, R. L. McCrory, D. D. Meyerhofer, and C. Cherfils-Clérouin, Phys. Plasmas **13**, 012702 (2006).

7. R. D. Petrasso, J. A. Frenje, C. K. Li, F. H. Séguin, J. R. Rygg, B. E. Schwartz, S. Kurebayashi, P. B. Radha, C. Stoeckl, J. M. Soures, J. Delettrez, V. Yu. Glebov, D. D. Meyerhofer, and T. C. Sangster, Phys. Rev. Lett. **90**, 095002 (2003).

8. J. A. Frenje, C. K. Li, F. H. Séguin, J. Deciantis, S. Kurebayashi, J. R. Rygg, R. D. Petrasso, J. Delettrez, V. Yu. Glebov, C. Stoeckl, F. J. Marshall, D. D. Meyerhofer, T. C. Sangster, V. A. Smalyuk, and J. M. Soures, Phys. Plasmas **11**, 2798 (2003).

9. T. R. Boehly, D. L. Brown, R. S. Craxton, R. L. Keck, J. P. Knauer, J. H. Kelly, T. J. Kessler, S. A. Kumpan, S. J. Loucks, S. A. Letzring, F. J. Marshall, R. L. McCrory, S. F. B. Morse, W. Seka, J. M. Soures, and C. P. Verdon, Opt. Commun. **133**, 495 (1997).

10. S. Skupsky and R. S. Craxton, Phys. Plasmas **6**, 2157 (1999).

11. H.-S. Bosch and G. M. Hale, Nucl. Fusion **32**, 611 (1992).

12. R. A. Lerche, D. W. Phillion, and G. L. Tietbohl, Rev. Sci. Instrum. **66**, 933 (1995).

13. F. H. Séguin, J. A. Frenje, C. K. Li, D. G. Hicks, S. Kurebayashi, J. R. Rygg, B.-E. Schwartz, R. D. Petrasso, S. Roberts, J. M. Soures, D. D. Meyerhofer, T. C. Sangster, J. P. Knauer, C. Sorce, V. Yu. Glebov, C. Stoeckl, T. W. Phillips, R. J. Leeper, K. Fletcher, and S. Padalino, Rev. Sci. Instrum. **74**, 975 (2003).

14. J. Delettrez, R. Epstein, M. C. Richardson, P. A. Jaanimagi, and B. L. Henke, Phys. Rev. A **36**, 3926 (1987).

15. Protons from the shell (ablator) material are accelerated by electrostatic fields while the laser pulse illuminates the capsule. These fields have decayed well before the time of nuclear production, several 100 ps after the end of the pulse, so they do not affect nuclear product spectra. See also D. G. Hicks, C. K. Li, F. H. Séguin, J. D. Schnittman, A. K. Ram, J. A. Frenje, R. D. Petrasso, J. M. Soures, D. D. Meyerhofer, S. Roberts, C. Sorce, C. Stoeckl, T. C. Sangster, and T. W. Phillips, Phys. Plasmas **8**, 606 (2001).

16. Comparison of absolute shock-bang times, which is timing with respect to the onset of the laser drive pulse, is quoted here. Comparison of the relative shock-bang times, with respect to the initial rise of compression burn, reveals that simulations predict shock-bang time to occur 12±15 ps early for 18-atm fills and 65±15 ps late for 3.6-atm fills.

17. C. K. Li, D. G. Hicks, F. H. Séguin, J. A. Frenje, R. D. Petrasso, J. M. Soures, P. B. Radha, V. Yu. Glebov, C. Stoeckl, D. R. Harding, J. P. Knauer, R. L. Kremens, F. J. Marshall, D. D. Meyerhofer, S. Skupsky, S. Roberts, C. Sorce, T. C. Sangster, T. W. Phillips, M. D. Cable, and R. J. Leeper, Phys. Plasmas **7**, 2578 (2000).

18. C. K. Li and R. D. Petrasso, Phys. Rev. Lett. **70**, 3059 (1993).

19. J. H. Gardner, D. L. Book, and I. B. Bernstein, J. Fluid Mech. **114**, 41 (1982).

20. J. R. Rygg, J. A. Frenje, C. K. Li, F. H. Séguin, R. D. Petrasso, F. J. Marshall, J. A. Delettrez, J. P. Knauer, D. D. Meyerhofer, and C. Stoeckl, "Observations of the Collapse of Asymmetrically Driven Convergent Spherical Shocks," manuscript in preparation (2007).

21. J. R. Rygg, J. A. Frenje, C. K. Li, F. H. Séguin, R. D. Petrasso, V. Yu. Glebov, D. D. Meyerhofer, T. C. Sangster, and C. Stoeckl, Phys. Rev. Lett. **98**, 215002 (2007).

22. O. Larroche, Eur. Phys. J. D **27**, 131 (2003).